

UKAEA-CCFE-PR(19)15

Pui-Wai Ma, S. L. Dudarev

# **Effect of stress on vacancy formation and migration in body-centred-cubic metals**

Enquiries about copyright and reproduction should in the first instance be addressed to the UKAEA Publications Officer, Culham Science Centre, Building K1/O/83 Abingdon, Oxfordshire, OX14 3DB, UK. The United Kingdom Atomic Energy Authority is the copyright holder.

The contents of this document and all other UKAEA Preprints, Reports and Conference Papers are available to view online free at [scientific-publications.ukaea.uk/](https://scientific-publications.ukaea.uk/)

# **Effect of stress on vacancy formation and migration in body-centred-cubic metals**

Pui-Wai Ma, S. L. Dudarev



# Effect of stress on vacancy formation and migration in body-centred-cubic metals

Pui-Wai Ma\* and S. L. Dudarev  
CCFE, UK Atomic Energy Authority, Culham Science Centre,  
Abingdon, Oxfordshire OX14 3DB, United Kingdom

Vacancy formation and migration control self-diffusion in pure crystalline materials, whereas irradiation produces high concentrations of vacancy and self-interstitial atom defects, exceeding by many orders of magnitude the thermal equilibrium concentrations. The defects themselves, and the extended dislocation microstructure formed under irradiation, generate strongly spatially fluctuating strain and stress fields. These fields alter the local formation and migration enthalpies of defects, and give rise to the anisotropy of diffusion even if in the absence of stress the diffusion tensor is isotropic. We have performed *ab initio* calculations of formation and migration energies of vacancies in all the commonly occurring body-centred-cubic (BCC) metals, including alkaline, alkaline-earth and transition metals, and computed elastic dipole and relaxation volume tensors of vacancies at the equilibrium lattice positions and along the vacancy migration pathways. We find that in all the BCC metals the dipole tensor of a migrating vacancy at a saddle point exhibits an anti-crowdion character. Applied external stresses or the local stresses generated by dislocations may enhance or suppress anisotropic diffusion by altering the energy barriers with respect to the direction of migration of a defect.

## I. INTRODUCTION

Vacancy formation and migration are the fundamental microscopic processes determining self-diffusion and atomic transport in crystalline materials [1]. At thermal equilibrium, vacancies are formed naturally by thermal fluctuations, whereas significantly higher concentrations of vacancies and self-interstitial atom (SIA) defects can be produced by irradiation [2, 3]. Elastic dipole and relaxation volume tensors of vacancies and self-interstitial atom defects computed from first principles at equilibrium lattice positions for a variety of BCC metals [4–6] show that for vacancies these tensors are entirely isotropic, whereas for SIA defects they are strongly anisotropic. Hence at an equilibrium lattice position, in the linear elasticity approximation a vacancy does not interact with a shear stress field even in an elastically anisotropic cubic material.

Dipole or relaxation volume tensors of a vacancy may acquire an anisotropic component if the vacancy is displaced from an equilibrium position, for example by a thermal fluctuation. At a relatively low temperature this has no fundamental effect on the nature of interaction with external elastic fields, as the dipole and relaxation volume tensors now become thermodynamic average quantities, with their symmetry still reflecting the cubic symmetry of the lattice site occupied by a vacancy. Large anisotropic distortions changing the symmetry of the dipole tensor may still arise from infrequent events associated with the migration of a vacancy from one lattice site to another. Using molecular statics, Sivak *et al.* [4] computed the elastic dipole tensor of a vacancy in iron at a saddle point between two equilibrium lattice positions, and showed that the distortion of the lattice around a vacancy at a saddle point resembled the distortion around a

(111) SIA crowdion defect, taken with the opposite sign. The anisotropic component of the dipole tensor resulting from this directional distortion now enables elastic interaction with a shear strain field, either applied externally or generated by other defects or dislocations. The strain and stress dependence of the migration enthalpy of a vacancy also gives rise to anisotropic diffusion in external elastic fields [7–10]. Strong external stresses and strains may also have an effect on the local vacancy concentration, promoting the migration of vacancies to the regions of high compressive strain.

Below, we explore how accurate electronic and atomic scale simulations can help generate high quality data required for the development of models for the diffusion-mediated dynamics of defects in the presence of deformation and stress. We briefly review the methods for computing the formation and migration energies as well as elastic dipole tensors  $P_{ij}$  and relaxation volume tensors  $\Omega_{ij}$  of defects using *ab initio* density functional theory (DFT). We then explore how the formation and migration enthalpies of defects change in the presence of external stresses or strains. We show that the relaxation volume tensor of a defect represents a particularly convenient parameter, describing the response of a defect to an external stress field.

The study below focuses on the DFT analysis of vacancy defects in several commonly occurring body-centred cubic (BCC) alkaline metals (Li, Na, K, Rb, Cs), an alkaline-earth metal (Ba), several non-magnetic transition metals (V, Nb, No, Ta, W), and two magnetic transition metals (Cr, Fe). We compare the calculated formation and migration energies with experimental values derived from self-diffusion experiments, and compare temperatures characterising the onset of migration of defects with temperatures of stage III resistivity recovery curves observed in materials exposed to electron irradiation at cryogenic temperatures. Using DFT supercell simulations, we compute elastic dipole tensor  $P_{ij}$  and re-

\* Leo.Ma@ukaea.uk

relaxation volume tensor  $\Omega_{ij}$  for a vacancy at equilibrium and at the saddle point on its migration trajectory. Calculations show that in all the metals investigated below, lattice distortions around a migrating vacancy exhibit anti-crowdion-like anisotropic character at all the intermediate positions along the transition pathway. The numerical values of elastic dipole tensors and relaxation volume tensors of defects derived from *ab initio* calculations enable accurate assessment of the effect of elastic fields on the generation and migration of vacancies in materials.

## II. BASIC FORMULAE

Methods for calculating formation energies of defects using periodic boundary conditions were recently reviewed in [5, 6, 11]. If a defect structure is simulated under the constraint of vanishing average strain, corresponding to the case where the translation vectors of the simulation cell remain fixed, the formation energy of the defect structure is given by the equation

$$E_D^F = E_D(N_D) - \frac{N_D}{N_{perf}} E_{perf}(N_{perf}) - E_{el}^{corr}, \quad (1)$$

where  $N_{perf}$  is the number of atoms in a perfect lattice cell,  $N_D$  is the number of atoms in a simulation box containing a defect, where for a vacancy  $N_D = N_{perf} - 1$ .  $E_D$  is the total energy of the cell containing a defect,  $E_{perf}$  is the energy of the perfect lattice cell, and  $E_{el}^{corr}$  is a correction term resulting from the condition of vanishing average strain and periodic boundary conditions. Procedures for evaluating  $E_{el}^{corr}$  are detailed in Refs. [5, 6, 11].

Migration energy  $E_D^M$  is the minimum energy required for a defect to move from one equilibrium position to another. Normally it is defined as the difference between the energy at the saddle point on the trajectory of migration and the energy at the nearest equilibrium position in the lattice.

$E_{el}^{corr}$  can be computed from the elastic dipole tensor  $P_{ij}$  of the defect and anisotropic elastic Green's function and its derivatives [12]. Elements of elastic dipole tensor can be evaluated from the macrostress  $\bar{\sigma}_{ij}$  that develops in a simulation cell due to the presence of a defect structure in it [5, 11, 13], namely

$$P_{ij} = - \int_V \sigma_{ij}^D dV = - \int_{V_{cell}} \sigma_{ij} dV = -V_{cell} \bar{\sigma}_{ij}. \quad (2)$$

Here  $\sigma_{ij}^D$  is the stress associated with a defect in an infinite medium subject to traction free boundary conditions [14], and  $\sigma_{ij}$  is the stress in a periodically translated simulation cell. Domain and Becquart [15] evaluated the dipole tensor of a vacancy at equilibrium from the Kanzaki forces, which converge if the simulation cell is sufficiently large [16]. Equation (2) applies to any cell size provided that atomic displacements at cell boundaries are well described by linear elasticity. In practice,

the accuracy of evaluation of  $P_{ij}$  from equation (2) is approximately 5%, assuming a typical size of the simulation cell used in *ab initio* calculations [5].

Assuming the experimental conditions involving applied constant external pressure  $p$ , we replace formation and migration energies of a defect by its formation and migration enthalpies [17]

$$H_D^{F/M} = E_D^{F/M} + p\Omega_D^{F/M}. \quad (3)$$

Formation and migration volumes of a defect  $\Omega_D^F$  and  $\Omega_D^M$  can be evaluated from its relaxation volume  $\Omega_{rel}$  computed at equilibrium and along the defect migration pathway. The relaxation volume tensor, proportional to the so-called  $\lambda$ -tensor [18], is related to the dipole tensor through the tensor of elastic compliance

$$\Omega_{ij} = S_{ijkl} P_{kl}. \quad (4)$$

The elastic compliance tensor  $\mathbf{S} = \mathbf{C}^{-1}$  is the inverse of the elastic constant tensor  $\mathbf{C}$ . The relaxation volume of a defect equals the trace of the relaxation volume tensor

$$\Omega_{rel} = \Omega_{11} + \Omega_{22} + \Omega_{33}. \quad (5)$$

The formation volume of a defect is related to its relaxation volume through

$$\Omega_D^F = \Omega_{rel}^{eq} + (N_{perf} - N_D)\Omega_0, \quad (6)$$

where  $\Omega_0$  is the atomic volume. For a vacancy  $\Omega_D^F = \Omega_{rel}^{eq} + \Omega_0$ . In all the cases investigated experimentally,  $\Omega_{rel}^{eq}$  is positive [17], implying that the total volume of a material always increases when vacancies are formed. Indeed, the formation of a vacancy in the bulk of a single crystal requires depositing an atom onto its surface. Despite the fact that the relaxation volume of a vacancy is negative [6] and the crystal lattice contracts when vacancies accumulate in the bulk of the material [19], the net result of vacancy formation is volume increase, since  $|\Omega_{rel}^{eq}| < \Omega_0$  [17].

The migration volume of a defect equals

$$\Omega_D^M = \Omega_D^{F,sd} - \Omega_D^{F,eq} = \Omega_{rel}^{sd} - \Omega_{rel}^{eq}. \quad (7)$$

Superscripts *sd* and *eq* refer to the saddle point and equilibrium configurations.

In anisotropic solids, instead of expressing defect formation and migration enthalpies in terms of pressure  $p$ , it is more appropriate to write them as functions of the stress tensor  $\sigma_{ij}$  describing the elastic field acting on a defect, namely

$$H_D^{F/M} = E_D^{F/M} - \sigma_{ij} \Omega_{ij}^{F/M}. \quad (8)$$

The formation volume tensor is therefore

$$\Omega_{ij}^F = \Omega_{ij}^{eq} + (N_{bulk} - N_D)\Omega_{0,ij} \quad (9)$$

where the second term is proportional to the atomic volume tensor. In a cubic crystal  $\Omega_{0,ij} = \frac{1}{3}\Omega_0\delta_{ij}$ . The migration volume tensor is therefore

$$\Omega_{ij}^M = \Omega_{ij}^{sd} - \Omega_{ij}^{eq}. \quad (10)$$

Returning to the relaxation volume tensor defined by equation (4) above, we note that depending on the specific application, it may be convenient to use either the relaxation volume tensor or the elastic dipole tensor when evaluating the energy of interaction between a defect and external elastic field [5]:

$$E_{el} = -\sigma_{ij}\Omega_{ij} = -C_{ijkl}\epsilon_{kl}S_{ijmn}P_{mn} = -\epsilon_{kl}P_{kl}. \quad (11)$$

Formation and migration energies, elastic dipole and relaxation volume tensors can be derived from the same set of DFT calculations.

There are two points that follow from the examination of Eq. (8). First, consider a case where a defect adopts several symmetry equivalent orientations in the lattice, all having the same energy. For example, a  $\langle 111 \rangle$  SIA has four equivalent degenerate orientations in a crystal lattice, where each orientation corresponds to the axis of the defect being parallel to one of the four  $\langle 111 \rangle$  type directions. In the presence of an external stress field, the formation enthalpy is going to vary as a function of the crystallographic orientation of the axis of the defect. This, for example, can bias the structure of an ensemble of interacting defects [20]. Also, stress fields can have a biasing effect on the diffusion of defects, through the direction-dependent contribution to the migration enthalpy, giving rise to the anisotropy of diffusion even in the nominally isotropic materials.

### III. FORMATION AND MIGRATION ENERGIES

All the *ab initio* DFT calculations described below were performed using Vienna Ab initio Simulation Package (VASP) [21–24]. We used simulation cells containing  $3 \times 3 \times 3$  bcc unit cells, or 54 atoms, in the perfect lattice configuration. Calculations were performed using a  $5 \times 5 \times 5$  k-point mesh and a plane wave cutoff energy that for Li was chosen at 1500 eV, for Na and K at 780 eV, for Rb and Cs at 660 eV, for Ba at 560 eV, and for all the other elements at 450 eV. Calculations were performed using PAW (Projector augmented-wave method) pseudo-potentials [25, 26] and the GGA-PBE (Perdew-Burke-Ernzerhof) [27, 28] exchange-correlation functional. There are 3, 7, 9, 9, 9 and 10 valence electrons per atom in Li, Na, K, Rb, Cs and Ba, respectively, and correspondingly 11, 12, 14, 11, 12, 11 and 12 valence electrons per atom in V, Cr, Fe, Nb, Mo, Ta and W. For all the elements we assumed a non-magnetic configuration, with the exception of Cr and Fe where we assumed a collinear magnetic ground state. Although the electronic ground state of Cr is believed to have the form of a spin density wave (SDW) [29], we adopt an anti-ferromagnetic (AFM) ground state in the current study, which has the energy indistinguishable from that of the SDW ground state within the error margin of *ab initio* calculations [30]. In the case of Fe, it is generally accepted that its ground state is collinear and ferromagnetic [31, 32].

Simulation cells containing 54 atoms in the perfect lattice configurations were relaxed to find the equilibrium lattice constant. Cell translation vectors then remained constant in all the subsequent calculations. Two distinct calculations of vacancy configurations for each element were performed by removing an atom from two different adjacent lattice sites displaced by one lattice vector in the  $[111]$  direction. In both calculations, ionic positions were fully relaxed. Then, nudge elastic band calculations [33, 34] were performed, to identify a vacancy migration trajectory, linking the two equilibrium vacancy configurations. For each element, a vacancy migration trajectory was represented by eleven configurational images. Convergence conditions required that the maximum force acting on an atom in a fully relaxed ionic configuration would not exceed 0.01 eV/Å.

To compute the relaxation volumes of defects, it is necessary to evaluate matrix elements of the tensor of elastic constants  $C_{ijkl}$ . This tensor is evaluated using the Le Page and Saxe method [35] for a 2 atom simulation cell and a  $30 \times 30 \times 30$  k-point mesh. The calculated values of elastic constants for all the elements are given in Table I together with experimental data.

Vacancy formation  $E_V^F$  and migration  $E_V^M$  energies derived from DFT calculations are given in Table II and Fig. 1. The sum of these energies  $E^{SD} = E_V^F + E_V^M$  gives the activation energy for self-diffusion [1]. The computed values compare favourably with the experimental data compiled by Ehrhart *et al.* [46]. For transition metals, the values given in Table II also compare well with results derived from earlier *ab initio* calculations [47, 48].

Experimental data for Li, Na, K, V, Nb, Ta, Cr, Mo, W and Fe show that the vacancy migration enthalpy scales linearly with the melting temperature of the material [49]. In alkaline metals, where melting temperatures are generally lower than those of transition metals, vacancy migration enthalpies are relatively small. Resistivity recovery experiments performed on electron irradiated elemental metals [46] show that in alkaline metals vacancies migrate at relatively low temperatures, corresponding to migration enthalpies of 0.038 eV, 0.03 eV and 0.038 eV in Li, Na and K, respectively. These values are at least an order of magnitude lower than vacancy migration enthalpies in transition metals. Our calculations confirm this.

Earlier *ab initio* calculation performed using local density approximation (LDA) show broadly similar results. For Li,  $E_V^F = 0.57$  eV (Ref. 50), 0.53 eV (Ref. 51), 0.54 eV (Ref. 52), 0.52 eV (Ref. 53), and  $E_V^M = 0.055$  eV (Ref. 53). For Na,  $E_V^F = 0.34$  eV (Ref. 54) and  $E_V^M = 0.054$  eV (Ref. 55). For K,  $E_V^F = 0.30$  eV (Ref. 55) and  $E_V^M = 0.051$  eV (Ref. 55). These LDA values are similar to those found in our GGA-PBE calculations. This is probably not surprising, as these simple metals do not exhibit effects of strong on-site electron correlations associated with localised *d* or *f* electrons. For completeness, in Table II we also provide data for Rb, Cs, and Ba, where the latter is an alkaline-earth metal. To the

	$C_{11}$ (GPa)	$C_{12}$ (GPa)	$C_{44}$ (GPa)	$\Omega_0$ ( $\text{\AA}^3$ )	$a_0$ ( $\text{\AA}$ )
Li	18.14	11.85	11.43	20.24	3.434
	<i>14.85<sup>a</sup></i>	<i>12.53<sup>a</sup></i>	<i>10.80<sup>a</sup></i>	<i>21.27<sup>b</sup></i>	<i>3.491<sup>b</sup></i>
Na	9.34	7.44	5.96	36.96	4.197
	<i>8.57<sup>c</sup></i>	<i>7.11<sup>c</sup></i>	<i>5.87<sup>c</sup></i>	<i>37.71<sup>b</sup></i>	<i>4.225<sup>b</sup></i>
K	3.91	3.44	2.70	73.66	5.282
	<i>4.17<sup>d</sup></i>	<i>3.41<sup>d</sup></i>	<i>2.86<sup>d</sup></i>	<i>71.32<sup>b</sup></i>	<i>5.225<sup>b</sup></i>
Rb	3.07	2.65	1.99	90.95	5.666
	<i>3.25<sup>e</sup></i>	<i>2.73<sup>e</sup></i>	<i>1.98<sup>e</sup></i>	<i>87.10<sup>b</sup></i>	<i>5.585<sup>b</sup></i>
Cs	2.16	1.85	1.38	116.75	6.158
	<i>2.47<sup>f</sup></i>	<i>2.06<sup>f</sup></i>	<i>1.48<sup>f</sup></i>	<i>110.45<sup>b</sup></i>	<i>6.045<sup>b</sup></i>
Ba	12.06	7.31	10.39	63.56	5.028
	<i>13.0<sup>g</sup></i>	<i>7.6<sup>g</sup></i>	<i>11.8<sup>g</sup></i>	<i>63.25<sup>b</sup></i>	<i>5.02<sup>b</sup></i>
V	279.59	142.02	26.72	13.43	2.995
	<i>227.9<sup>h</sup></i>	<i>118.7<sup>h</sup></i>	<i>42.6<sup>h</sup></i>	<i>13.91<sup>b</sup></i>	<i>3.03<sup>b</sup></i>
Nb	248.76	135.24	19.46	18.32	3.322
	<i>246.6<sup>h</sup></i>	<i>133.2<sup>h</sup></i>	<i>28.1<sup>h</sup></i>	<i>17.97<sup>b</sup></i>	<i>3.30<sup>b</sup></i>
Mo	469.07	157.72	99.71	15.77	3.159
	<i>464.7<sup>h</sup></i>	<i>161.5<sup>h</sup></i>	<i>108.9<sup>h</sup></i>	<i>15.63<sup>b</sup></i>	<i>3.15<sup>b</sup></i>
Ta	266.28	161.36	76.75	18.27	3.319
	<i>266.0<sup>h</sup></i>	<i>161.2<sup>h</sup></i>	<i>82.4<sup>h</sup></i>	<i>17.97<sup>b</sup></i>	<i>3.30<sup>b</sup></i>
W	518.26	199.77	142.09	16.15	3.185
	<i>522.4<sup>h</sup></i>	<i>204.4<sup>h</sup></i>	<i>160.6<sup>h</sup></i>	<i>15.78<sup>b</sup></i>	<i>3.16<sup>b</sup></i>
Cr	448.12	62.03	102.13	11.72	2.862
	<i>394.1<sup>i</sup></i>	<i>88.5<sup>i</sup></i>	<i>103.75<sup>i</sup></i>	<i>11.94<sup>b</sup></i>	<i>2.88<sup>b</sup></i>
Fe	289.34	152.34	107.43	11.36	2.832
	<i>243.1<sup>j</sup></i>	<i>138.1<sup>j</sup></i>	<i>121.9<sup>j</sup></i>	<i>11.82<sup>b</sup></i>	<i>2.87<sup>b</sup></i>

<sup>a</sup>Ref. 36, <sup>b</sup>Ref. 37, <sup>c</sup>Ref.38, <sup>d</sup>Ref. 39, <sup>e</sup>Ref. 40, <sup>f</sup>Ref. 41, <sup>g</sup>Ref. 42, <sup>h</sup>Ref. 43, <sup>i</sup>Ref. 44, <sup>j</sup>Ref. 45.

TABLE I. Elastic constants (GPa) are calculated following the Le Page and Saxe [35] method, using a 2-atom cell and  $30 \times 30 \times 30$  k-points. Atomic volumes ( $\text{\AA}^3$ ) and lattice constants ( $\text{\AA}$ ) are computed using 54 atom perfect lattice simulation cell. Entries given in italics are the experimentally observed values.

best of our knowledge, there are no prior experimental or theoretical results available for these metals.

Assuming that the temperature of stage III,  $T(\text{III})$ , of recovery of electron irradiated materials corresponds to the onset of vacancy migration, we can estimate the vacancy migration temperature  $T^M$  from the classical transition state theory [56]. The effective migration event frequency can be written as

$$\nu = \nu_0 \exp(-E^M/k_B T), \quad (12)$$

where  $\nu_0$  is the vacancy migration attempt frequency. The value of  $\nu_0$  can be estimated from the Debye frequency and the corresponding Debye temperature  $\theta_D$ . Choosing  $\nu = 1\text{s}^{-1}$  as a characteristic timescale of experimental observations, we can estimate  $T^M$  and compare it with the temperature  $T(\text{III})$  of stage III of resistivity recovery as shown in Table III.

	$E_V^F$	$E_V^M$	$E^{SD}$
Li	0.506	0.053	0.559
	<i>0.480</i>	<i>0.038</i>	<i>0.518</i>
Na	0.334	0.053	0.387
	<i>0.335</i>	<i>0.030</i>	<i>0.365</i>
K	0.292	0.053	0.345
	<i>0.34</i>	<i>0.038</i>	<i>0.386</i>
Rb	0.261	0.046	0.306
Cs	0.249	0.047	0.296
Ba	1.009	0.216	1.225
V	2.553	0.650	3.203
	<i>2.1-2.2</i>	<i>0.5</i>	<i>2.6-3.21</i>
Nb	2.715	0.646	3.361
	<i>2.6-3.07</i>	<i>0.55</i>	<i>3.62</i>
Mo	2.830	1.159	3.988
	<i>3.0-3.24</i>	<i>1.35-1.62</i>	<i>4.53</i>
Ta	2.951	0.761	3.711
	<i>2.2-3.1</i>	<i>0.7</i>	<i>3.8-4.39</i>
W	3.354	1.729	5.083
	<i>3.51-4.1</i>	<i>1.70-2.02</i>	<i>5.45</i>
Cr	3.015	1.105	4.120
	<i>2.0-2.27</i>	<i>0.95</i>	<i>4.58</i>
Fe	2.370	0.682	3.052
	<i>1.59-2.0</i>	<i>0.55</i>	<i>2.36-3.01</i>

TABLE II. Calculated vacancy formation energy  $E_V^F$  (eV), vacancy migration energy  $E_V^M$  (eV), and the self-diffusion activation energy  $E^{SD}$  (eV). Experimental data are given in italics below the calculated values. Experimental values of  $E_V^F$ ,  $E_V^M$  and  $E^{SD}$  are taken from Ref. 46.

element	$\theta_D$ (K)	Est. $T^M$ (K)	Exp. $T(\text{III})$ (K)
Li	344	29.4	16.5
Na	158	20.1	15-15.5
K	91	20.4	14-16
Rb	56	17.9	–
Cs	38	18.6	–
Ba	110	82.7	–
V	380	239.2	170
Nb	275	240.0	200-270
Mo	450	424.1	400-640
Ta	240	284.0	260-300
W	400	635.2	620-900
Cr	630	400.1	350
Fe	470	249.4	220-278

TABLE III. Estimated temperature of vacancy migration  $T^M$  (K) compared to the temperature of stage III resistivity recovery observed in elemental metals irradiated by high energy electrons at cryogenic temperatures. Debye temperature values  $\theta_D$  (K) are taken from Ref. 37. Values of stage III resistivity recovery temperatures are taken from Ref. 46.



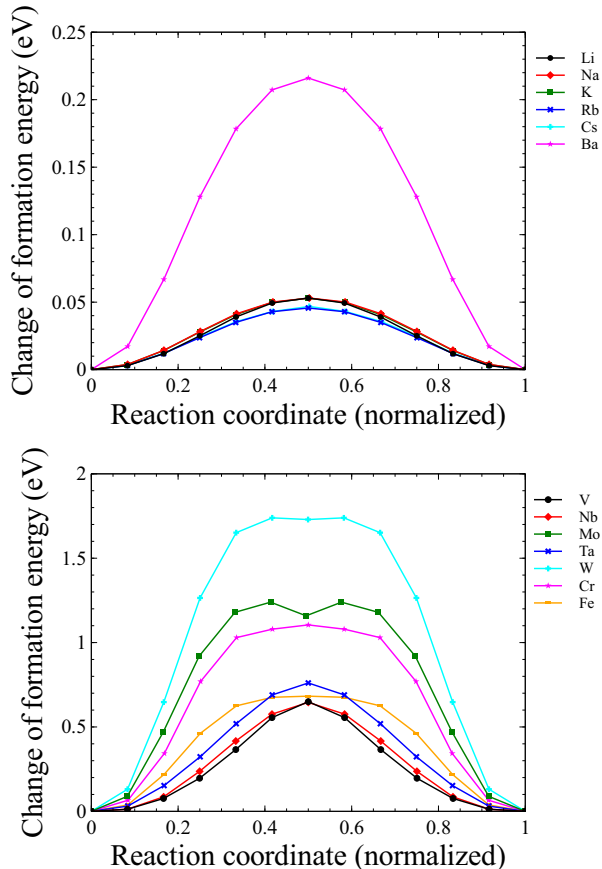


FIG. 1. (Color online) Energy of a mono-vacancy at various points along the vacancy migration pathway. Values indicated by symbols on the graphs were derived from nudged elastic band calculations involving eleven images and spanning the interval between two adjacent equilibrium positions of a vacancy in bcc lattice.

#### IV. ELASTIC DIPOLE AND RELAXATION VOLUME TENSORS

We now proceed to the calculation of dipole tensors  $P_{ij}$  of vacancies at equilibrium and in transition state configurations. Fig. 2 shows how the diagonal  $P_{ii}$  and off-diagonal  $P_{ij}$ ,  $i \neq j$ , elements of the elastic dipole tensor vary along the vacancy migration pathway. The diagonal elements of the dipole tensor  $P_{ii}$  are all negative, and they vary in such a way that no particular trend can be observed. The off-diagonal terms, all acquire negative values on the migration trajectory. The result is similar to the one found by Sivak *et al.* [4] in iron for the saddle point on the vacancy transition pathway, investigated using molecular statics.

To gain better insight into the nature of electronic processes associated with vacancy migration, we inspected electronic density configurations characterising vacancy migration. Figures 3 to 6 show two-dimensional plots of electron charge density difference computed for Li, Na, V and W. As the atomic size increases, and the character

of bonding changes from that mediated by  $s$  electrons in alkaline metals to  $d$  electrons in transition metals, the pattern changes. The picture of density transformation is particularly simple in Li, whereas in tungsten we observe significant effects of directionality of interatomic bonding associated with  $5d$  electrons. Still, the pattern of variation of charge density deformation from the equilibrium to the saddle point on the trajectory of vacancy migration remains broadly similar. In all the bcc metals, an atom exchanges its position with a vacancy, and this does not involve the formation of any collective string-like configuration typically associated with a self-interstitial crowdion defect [48, 57, 58]. Still, the elastic dipole tensor of a migrating vacancy exhibits the same symmetry and character as an “anti-crowdion” for all the metals explored in this study.

Using equations 4 to 7, we evaluate relaxation volume tensors, formation and migration volumes of vacancies in all the metals included in this study. The values are summarised in Table IV. Experimental information on vacancy formation and relaxation volumes is relatively limited, still we know that the experimentally measured values of vacancy formation volume in noble metals vary between 0.5 and 0.7 atomic volume [17], and the relaxation volume of a vacancy is negative [19].

Comparing the values predicted by our calculations to earlier *ab initio* results derived using LDA for Li, Na and K, we find similar magnitudes of parameters  $\Omega_V^F$  and  $\Omega_V^M$ . For Li, values predicted earlier are  $\Omega_V^F = 0.52\Omega_0$  (Ref. 51),  $0.49\Omega_0$  (Ref. 52),  $0.49\Omega_0$  at 0GPa and  $0.36\Omega_0$  at 3.4GPa (Ref. 59), and  $\Omega_V^M = -0.2\Omega_0$  at 0GPa and  $-0.06\Omega_0$  at 3.4GPa (Ref. 59). For Na, the literature values are  $\Omega_V^F = 0.51\Omega_0$  (Ref. 54),  $0.5\Omega_0$  at 0GPa and  $0.29\Omega_0$  at 2.8GPa (Ref. 59), and  $\Omega_V^M = -0.1\Omega_0$  at 0GPa and  $-0.01\Omega_0$  at 2.8GPa (Ref. 59). For K, earlier calculations give  $\Omega_V^F = 0.45\Omega_0$  (Ref. 55). These values are in good agreement with the values found in the present study. We see that the migration volume of a vacancy is relatively small, with the exception of the case of Cr. Our calculations complement the data not available in literature, and also show how the relaxation volume tensor varies during vacancy migration.

#### V. STRESS-INDUCED ANISOTROPIC DIFFUSION

All the off-diagonal elements of elastic dipole tensor  $P_{ij}$  of a vacancy vanish at an equilibrium position. However, whenever a vacancy is moving away from its equilibrium position, the off-diagonal elements of  $P_{ij}$  are non-zero. Figs. 2 and 7 show how both tensors vary as a vacancy moves from one equilibrium position in the lattice to another.

We have already observed that the elastic dipole and relaxation volume tensors of a vacancy at a saddle point resemble those of a  $\langle 111 \rangle$  SIA defect, but with an opposite sign. For a vacancy at a saddle point or for a  $\langle 111 \rangle$  SIA

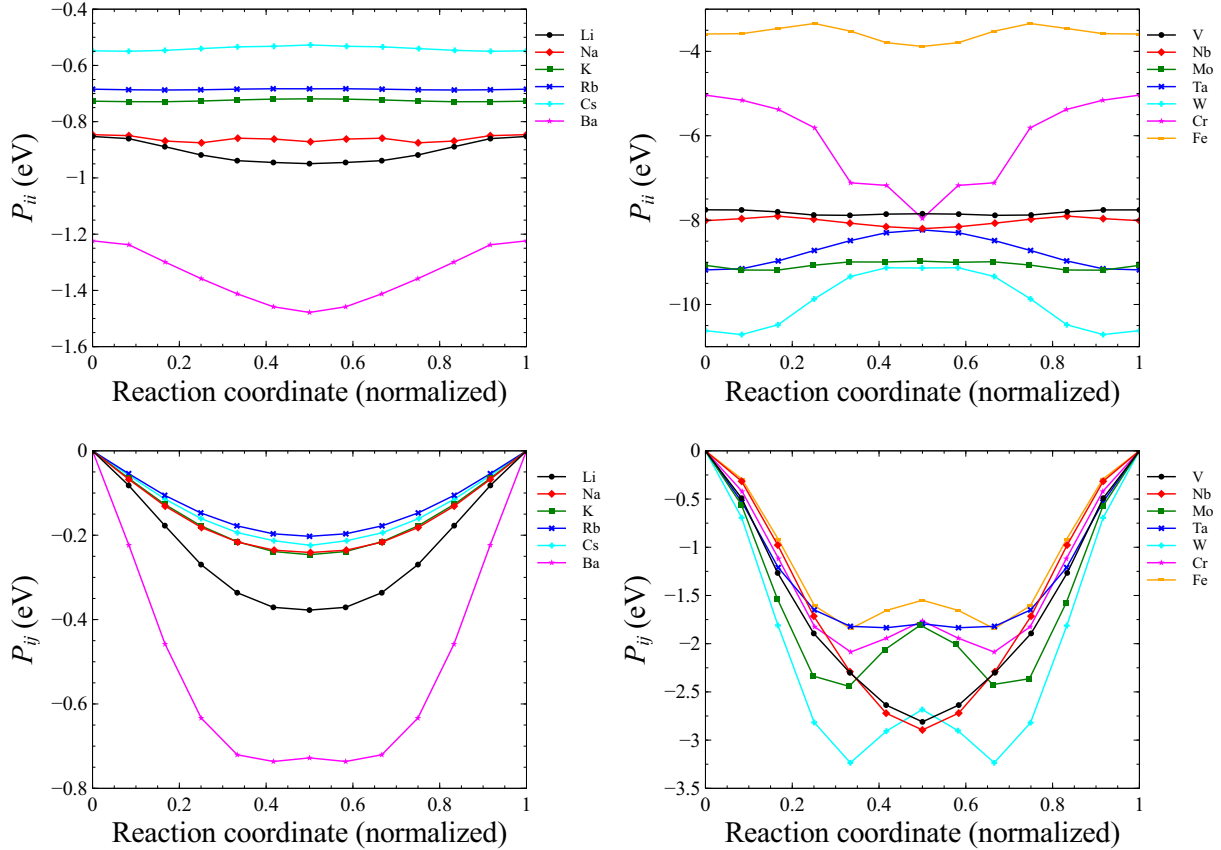


FIG. 2. (Color online) Variation of the elastic dipole tensor of a vacancy along its migration pathway linking two adjacent equilibrium positions in bcc lattice.  $P_{ii}$  is a diagonal element of the dipole tensor (note that  $P_{11} = P_{22} = P_{33}$ ), whereas  $P_{ij}$  is an off-diagonal element (where  $P_{12} = P_{23} = P_{13}$  for a transition in the  $[111]$  direction). The values are given in eV units.

defect, there are four symmetry-equivalent and energy-degenerate orientations, namely  $[111]$ ,  $[\bar{1}11]$ ,  $[1\bar{1}1]$  and  $[11\bar{1}]$ . The diagonal elements of  $P_{ij}$  for all these orientations are the same, however the off-diagonal elements differ. If we take the elastic dipole tensor of a defect in the  $[111]$  orientation as

$$P_{ij}^{[111]} = P_{ij}^{[\bar{1}\bar{1}\bar{1}]} = \begin{pmatrix} P_a & P_b & P_b \\ P_b & P_a & P_b \\ P_b & P_b & P_a \end{pmatrix}, \quad (13)$$

then the elastic dipole tensors for the other three orientations have the form

$$P_{ij}^{[\bar{1}11]} = P_{ij}^{[1\bar{1}\bar{1}]} = \begin{pmatrix} P_a & -P_b & -P_b \\ -P_b & P_a & P_b \\ -P_b & P_b & P_a \end{pmatrix}, \quad (14)$$

$$P_{ij}^{[11\bar{1}]} = P_{ij}^{[\bar{1}\bar{1}1]} = \begin{pmatrix} P_a & -P_b & P_b \\ -P_b & P_a & -P_b \\ P_b & -P_b & P_a \end{pmatrix}, \quad (15)$$

$$P_{ij}^{[11\bar{1}]} = P_{ij}^{[\bar{1}\bar{1}1]} = \begin{pmatrix} P_a & P_b & -P_b \\ P_b & P_a & -P_b \\ -P_b & -P_b & P_a \end{pmatrix}. \quad (16)$$

The magnitude of the off-diagonal elements does not change, but the sign changes depending on the choice of the direction of axis of the defect.

There are eight equivalent nearest neighbour positions in bcc lattice where a vacancy can hop from a given lattice site. A vacancy can jump left or right along any of the four directions, i.e.  $[111]$ ,  $[\bar{1}11]$ ,  $[1\bar{1}1]$ , and  $[11\bar{1}]$ . Whenever there is an external stress, migration enthalpy differs depending on the choice of direction in which a vacancy performs a hop.

Consider vanadium as an example. If a shear stress of  $\sigma_{12} = \sigma_{21} = 0.5 \text{ GPa}$  is imposed, as illustrated in Fig. 9, the migration enthalpy for a hop in the  $[111]$  direction decreases by about 0.05 eV, whereas the migration enthalpy in the  $[\bar{1}\bar{1}\bar{1}]$  direction increases by about 0.05 eV. Considering all the four possible directions of vacancy migration, we find that a vacancy moves easier in the  $[111]$  and  $[11\bar{1}]$  directions, compared to the  $[\bar{1}\bar{1}\bar{1}]$  and  $[1\bar{1}1]$  directions, if the material is subjected to shear stress  $\sigma_{12} > 0$ .

A more rigorous way of treating the effect of stress on

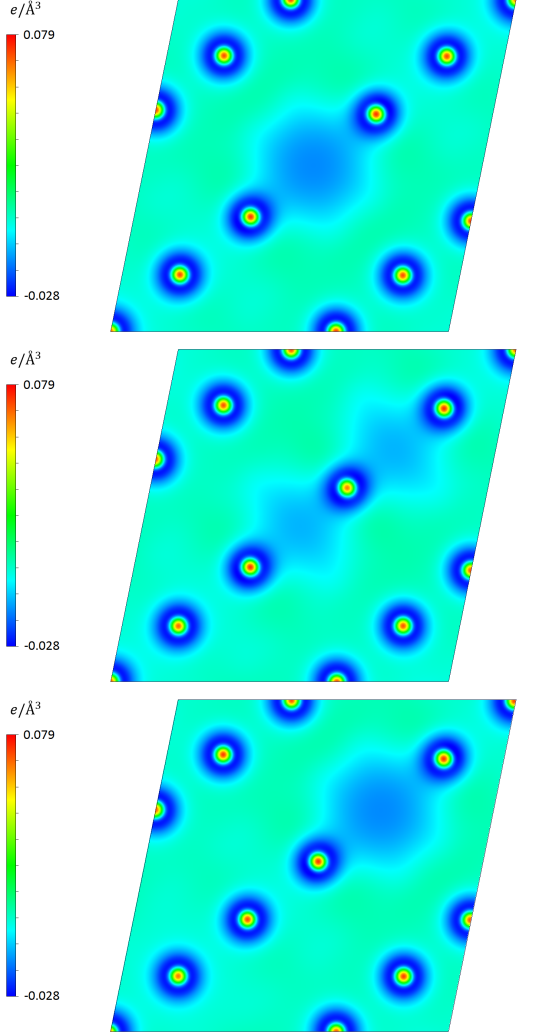


FIG. 3. (Color online) Two-dimensional plot of electron charge density difference computed for Li in the (211) plane. The plot refers to a vacancy migrating from one equilibrium lattice position to another along the [111] direction. (Top) the initial equilibrium position, (Middle) the saddle point, and (Bottom) the final equilibrium position. Electron charge density difference is defined as the ground state electron density computed for a given configuration of atoms minus the superposition of atomic charge densities.

vacancy diffusion is provided by the formalism of anisotropic diffusion tensor. Following Dederichs and Schroeder [9], we write the anisotropic diffusion tensor of a vacancy moving in an applied strain field as

$$D_{ij}(\mathbf{R}) = \frac{1}{2} \sum_h \lambda_h r_i^h r_j^h \exp\left(\frac{\epsilon_{kl}(\mathbf{R})(P_{kl}^{sd,h} - P_{kl}^{eq})}{k_B T}\right), \quad (17)$$

where  $\lambda_h = \nu_0 \exp(-\beta E_D^{M,h})$ , index  $h$  refers to a possible hopping site, and  $r_i^h$  is a Cartesian component of the hopping direction vector. In the limit where the applied strain field is relatively small, the exponential factor in

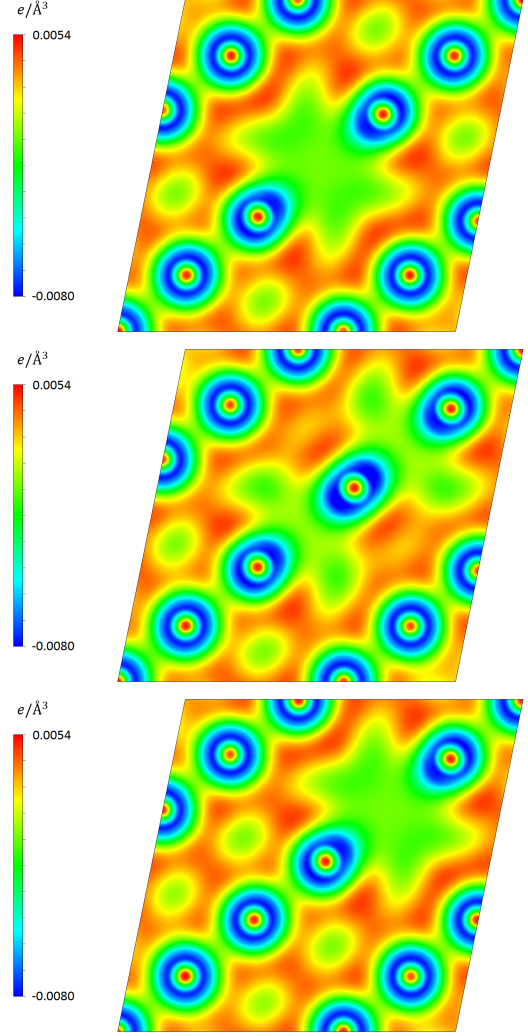


FIG. 4. (Color online) Two-dimensional plot of electron charge density difference computed for Na in the (211) plane. The plot refers to a vacancy migrating from one equilibrium lattice position to another along the [111] direction. (Top) the initial equilibrium position, (Middle) the saddle point, and (Bottom) the final equilibrium position.

equation (17) can be expanded in the Taylor series, where by retaining only the linear terms we obtain

$$D_{ij}(\mathbf{R}) \approx D_{ij,0} + d_{ijkl} \epsilon_{kl}(\mathbf{R}), \quad (18)$$

where the diffusion constant tensor

$$D_{ij,0} = \frac{1}{2} \sum_h \lambda_h r_i^h r_j^h, \quad (19)$$

describes diffusion in the absence of applied field, and  $d_{ijkl}$  is the elasto-diffusion tensor [9]:

$$d_{ijkl} = \frac{1}{2} \sum_h \lambda_h r_i^h r_j^h \left(\frac{P_{kl}^{sd} - P_{kl}^{eq}}{k_B T}\right). \quad (20)$$

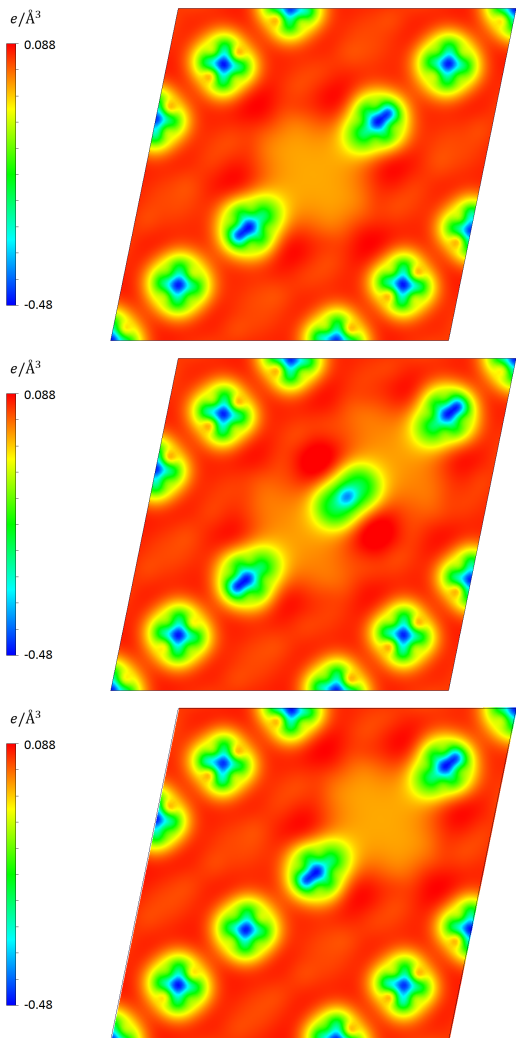


FIG. 5. (Color online) Two-dimensional plot of electron charge density difference computed for V in the (211) plane. The plot refers to a vacancy migrating from one equilibrium lattice position to another along the [111] direction. (Top) the initial equilibrium position, (Middle) the saddle point, and (Bottom) the final equilibrium position.

We note that linear in applied field expansion applies only in the limit where the argument of the exponential function is small.

Alternatively, the anisotropic diffusion tensor can be expressed in terms of the migration volume tensor and the stress tensor, see equation (11), namely

$$D_{ij}(\mathbf{R}) = \frac{1}{2} \sum_h \lambda_h r_i^h r_j^h \exp\left(\frac{\sigma_{kl}(\mathbf{R})(\Omega_{kl}^{M,h} - \Omega_{kl}^{eq})}{k_B T}\right). \quad (21)$$

Using this equation and the data given in the Tables, we can give an estimation to the variation of  $D_{ij}$  under applied stress. For a vacancy migrating in a cubic lattice,

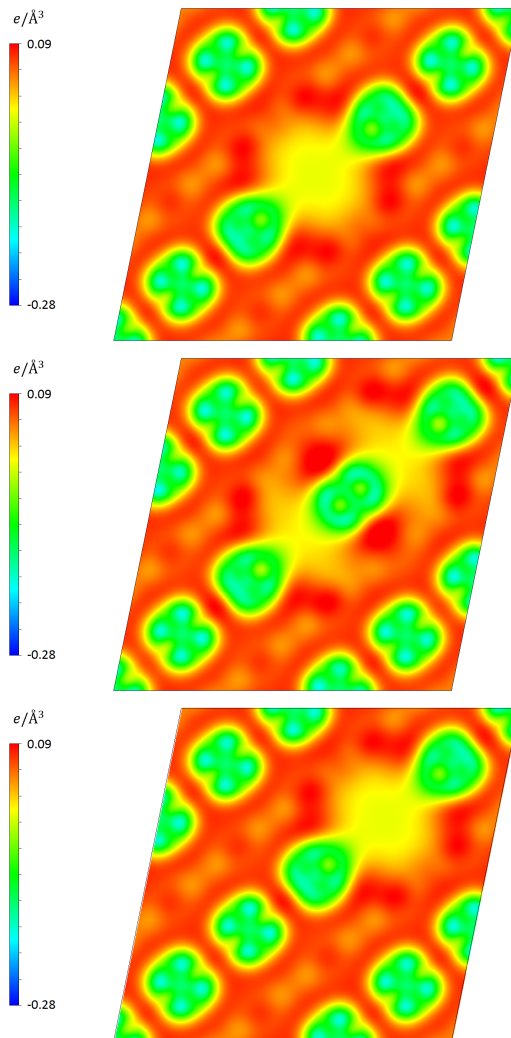


FIG. 6. (Color online) Two-dimensional plot of electron charge density difference computed for W in the (211) plane. The plot refers to a vacancy migrating from one equilibrium lattice position to another along the [111] direction. (Top) the initial equilibrium position, (Middle) the saddle point, and (Bottom) the final equilibrium position.

we write

$$D_{ij} = \frac{\lambda}{2} \left(\frac{a}{2}\right)^2 X_{ij}, \quad (22)$$

where

$$X_{ij} = \sum_h e_i^h e_j^h \exp\left(\frac{\sigma_{kl}(\mathbf{R})(\Omega_{kl}^{M,h} - \Omega_{kl}^{eq})}{k_B T}\right). \quad (23)$$

is an auxiliary dimensionless diffusion tensor, and  $\mathbf{e}^h = \mathbf{r}^h/(a/2)$ . We note that components of vector  $e_i^h$  take values of +1 or -1. Under stress-free conditions, equation (21) correctly reproduces the isotropic case where the diffusion constant tensor is diagonal  $D_{ij} = D_0 \delta_{ij}$ ,

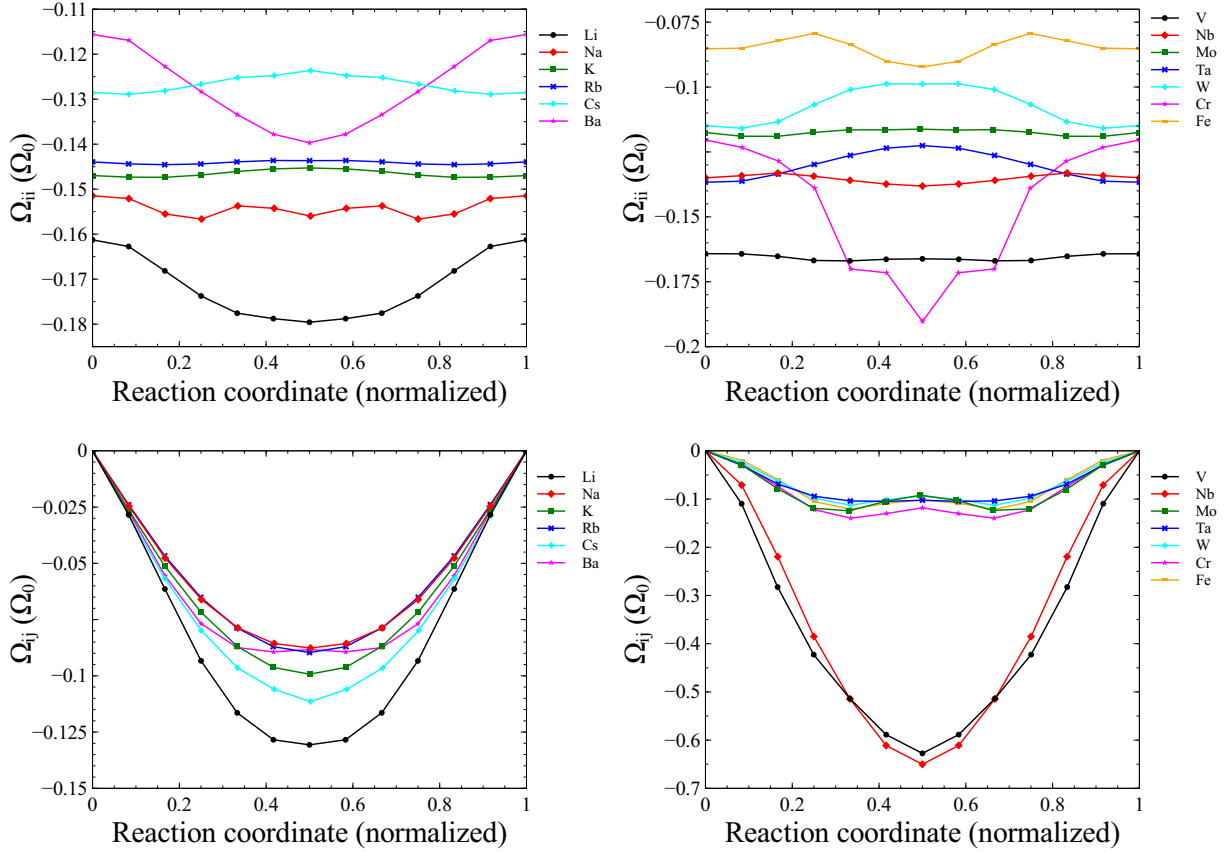


FIG. 7. (Color online) Variation of the relaxation volume tensor of a vacancy along its migration pathway.  $\Omega_{ii}$  is a diagonal element of the relaxation volume tensor (note that  $\Omega_{11} = \Omega_{22} = \Omega_{33}$ ), whereas  $\Omega_{ij}$  is an off-diagonal element (where  $\Omega_{12} = \Omega_{23} = \Omega_{13}$  for a transition in the  $[111]$  direction). The values are given in atomic volume units  $\Omega_0$ .

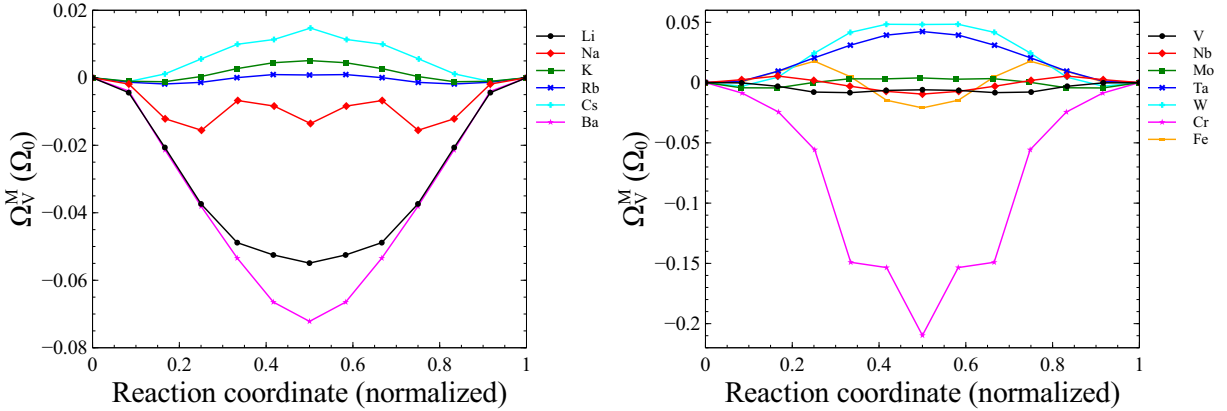


FIG. 8. (Color online) Variation of the migration volume of a vacancy along the transition pathway between two equilibrium positions of a vacancy in bcc lattice. The values are given in atomic volume units  $\Omega_0$ .

and

$$D_0 = \frac{Zl^2\lambda}{2d} \quad (24)$$

where  $Z = 8$  is number of nearest neighbour positions accessible to a direct vacancy hop,  $l = \sqrt{3}a/2$  is the hopping

distance, and  $d = 3$  is the number of spatial dimensions.

Consider vanadium and tungsten as examples. Assuming realistic applied shear stress of  $\sigma_{12} = \sigma_{21} = 0.1\text{GPa}$  or  $0.5\text{GPa}$ , and temperatures of  $500\text{K}$ ,  $800\text{K}$  and  $1000\text{K}$ , we compute elements of the dimensionless auxiliary dif-

	$P_{ii}(\text{eq})$	$P_{ii}(\text{sd})$	$P_{ij}(\text{sd})$	$\Omega_{ii}(\text{eq})$	$\Omega_{ii}(\text{sd})$	$\Omega_{ij}(\text{sd})$
Li	-0.853	-0.949	-0.378	-0.161	-0.180	-0.131
Na	-0.846	-0.871	-0.241	-0.151	-0.156	-0.088
K	-0.727	-0.719	-0.246	-0.147	-0.145	-0.099
Rb	-0.684	-0.683	-0.203	-0.144	-0.144	-0.090
Cs	-0.548	-0.527	-0.224	-0.129	-0.124	-0.111
Ba	-1.224	-1.478	-0.728	-0.116	-0.140	-0.088
V	-7.756	-7.850	-2.811	-0.164	-0.166	-0.628
Nb	-8.013	-8.202	-2.895	-0.135	-0.138	-0.650
Mo	-9.072	-8.972	-1.808	-0.118	-0.116	-0.092
Ta	-9.181	-8.232	-1.794	-0.137	-0.123	-0.102
W	-10.621	-9.135	-2.683	-0.115	-0.099	-0.094
Cr	-5.037	-7.962	-1.764	-0.120	-0.190	-0.118
Fe	-3.589	-3.883	-1.549	-0.085	-0.092	-0.102

TABLE IV. Diagonal and off-diagonal elements of elastic dipole and relaxation volume tensors of a vacancy at an equilibrium position and in a saddle point configuration. Elements of the elastic dipole tensor are given in eV units, whereas the values of relaxation volume tensors are given in atomic volume units  $\Omega_0$ . Indexes  $ii$  refer to a diagonal elements of the tensor, whereas  $ij$  refer to an off-diagonal element. The diagonal elements are the same, and so are the off-diagonal elements, of both tensors. The off-diagonal elements of elastic dipole and relaxation volume tensors vanish if the vacancy is at an equilibrium position. A saddle point corresponds to the middle of the transition pathway. Note that this point may not necessarily correspond to the highest energy on the transition pathways, as it is the case in Mo and W. The relaxation volume of a vacancy equals the sum of diagonal elements of the relaxation volume tensor  $\Omega_{rel} = \Omega_{11} + \Omega_{22} + \Omega_{33}$ .

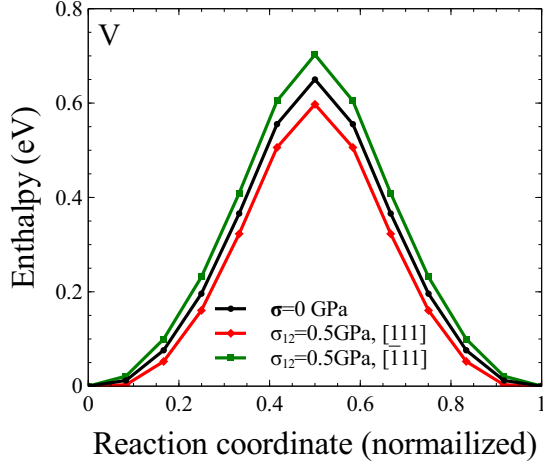


FIG. 9. (Color online) Variation of the migration enthalpy of a vacancy along the migration pathway in the absence of applied stress, and under shear stress of  $\sigma_{12} = \sigma_{21} = 0.5\text{GPa}$ , computed for the hopping trajectories extending in the  $[111]$  and  $[\bar{1}11]$  directions.

	$\Omega_{rel}^{eq}$	$\Omega_V^F$	$\Omega_V^M$	$\Omega^{SD}$	$p^{SF}$
Li	-0.484	0.516	-0.05491	0.461	-7.76
Na	-0.454	0.546	-0.01356	0.532	-2.65
K	-0.441	0.559	0.00509	0.564	-1.14
Rb	-0.432	0.568	0.00082	0.569	-0.81
Cs	-0.386	0.614	0.01472	0.629	-0.56
Ba	-0.347	0.653	-0.07219	0.581	-3.89
V	-0.493	0.507	-0.00595	0.502	-60.14
Nb	-0.405	0.595	-0.00955	0.586	-39.88
Mo	-0.353	0.647	0.00390	0.651	-44.39
Ta	-0.410	0.590	0.04236	0.632	-43.80
W	-0.345	0.655	0.04821	0.704	-50.79
Cr	-0.361	0.639	-0.20973	0.429	-64.53
Fe	-0.256	0.744	-0.02098	0.723	-44.97

TABLE V. Vacancy relaxation volume at equilibrium  $\Omega_{rel}^{eq}$ , vacancy formation volume  $\Omega_V^F$ , vacancy migration volume  $\Omega_V^M$ , and self-diffusion volume  $\Omega^{SD}$  computed using density functional theory, see text. The values are given in atomic volume units  $\Omega_0$ . Experimental data, where available, are given in italics below the computed values. Experimental values of  $\Omega^{SD}$  for <sup>a</sup>Ref. 60 and <sup>b</sup>Ref. 61 are the self-diffusion activation volumes. Experimental values of vacancy formation volumes are from <sup>c</sup>Ref. 46. Critical pressure required for the spontaneous formation of a vacancy  $p^{SF}$  is calculated according to Eq. (3) and is given in GPa units.

0.1GPa	$X_{ii}$	$X_{12} = X_{21}$	0.5GPa	$X_{ii}$	$X_{12} = X_{21}$
500K	8.24	-1.97	500K	14.75	-12.39
800K	8.09	-1.23	800K	10.45	-6.72
1000K	8.06	-0.98	1000K	9.54	-5.20

TABLE VI. Elements of the auxiliary diffusion tensor  $X_{ij}$  computed for Vanadium assuming the shear stress of  $\sigma_{12} = \sigma_{21} = 0.1\text{GPa}$  and  $0.5\text{GPa}$ , and temperatures of 500K, 800K and 1000K. The auxiliary diffusion tensor is defined by equation (22). Elements of  $X_{ij}$  not given in the table vanish due to symmetry.

0.1GPa	$X_{ii}$	$X_{12} = X_{21}$	0.5GPa	$X_{ii}$	$X_{12} = X_{21}$
500K	8.01	-0.315	500K	8.19	-1.773
800K	8.00	-0.220	800K	8.08	-1.103
1000K	8.00	-0.176	1000K	8.05	-0.881

TABLE VII. Elements of the auxiliary diffusion tensor  $X_{ij}$  computed for Tungsten assuming the shear stress of  $\sigma_{12} = \sigma_{21} = 0.1\text{GPa}$  and  $0.5\text{GPa}$ , and temperatures of 500K, 800K and 1000K. The auxiliary diffusion tensor is defined by equation (22). Elements of  $X_{ij}$  not given in the table vanish due to symmetry.

fusion tensor  $X_{ij}$ , and summarise the results in Tables VI and VII. Other elements of  $X_{ij}$  not listed in the Tables vanish due to symmetry. We note that although at equilibrium, where the relaxation volume tensor is isotropic and a vacancy does not interact with the shear component of the applied stress, the effect of stress on vacancy diffusion can be fairly significant. Furthermore, the fact that a shear stress can influence vacancy migration shows that vacancy diffusion may be affected not only by elastic fields of edge dislocations [62, 63], but also by the elastic fields of screw dislocations where the stress field is dominated by its shear components.

## VI. CONCLUSION

We have evaluated vacancy migration and formation energies for a number of bcc metals including alkaline, alkaline-earth and transition metals. We have also evaluated elastic dipole tensors and relaxation volume tensors of vacancies at equilibrium and on trajectories of migration. We find that since the off-diagonal elements of both elastic dipole and relaxation volume tensors of a migrating vacancy do not vanish, diffusion of vacancies can be

significantly affected by shear stress fields, either applied externally or generated by other defects and dislocations. In particular, the fact that migration barriers in different directions change due to the interaction with external stress, can give rise to anisotropic diffusion. This phenomenon is described by the anisotropic diffusion tensor, which can be readily computed from the *ab initio* data generated and compiled in this study.

## ACKNOWLEDGMENTS

This work has been carried out within the framework of the EUROfusion Consortium and has received funding from the Euratom research and training programme 2014-2018 and 2019-2020 under grant agreement No 633053 and from the RCUK Energy Programme [grant number EP/P012450/1]. To obtain further information on the data and models underlying this paper please contact PublicationsManager@ukaea.uk. The views and opinions expressed herein do not necessarily reflect those of the European Commission. We also acknowledge EUROfusion for the provision of access to Marconi supercomputer facility at CINECA in Italy.

- 
- [1] A. R. Allnatt and A. B. Lidiard, *Atomic Transport in Solids* (Cambridge University Press, Cambridge, UK, 2003) p. 572.
  - [2] A. E. Sand, K. Nordlund, and S. L. Dudarev, “Radiation damage production in massive cascades initiated by fusion neutrons in tungsten,” *Journal of Nuclear Materials* **455**, 207–211 (2014), proceedings of the 16th International Conference on Fusion Reactor Materials (ICFRM-16).
  - [3] A. E. Sand, M. J. Aliaga, M. J. Caturla, and K. Nordlund, “Surface effects and statistical laws of defects in primary radiation damage: Tungsten vs. iron,” *Europhysics Letters* **115**, 36001 (2016).
  - [4] A. B. Sivak, V. A. Romanov, and V. M. Chernov, “Diffusion of self-point defects in body-centered cubic iron crystal containing dislocations,” *Crystallography Reports* **55**, 97–108 (2010).
  - [5] S. L. Dudarev and Pui-Wai Ma, “Elastic fields, dipole tensors, and interaction between self-interstitial atom defects in bcc transition metals,” *Phys. Rev. Materials* **2**, 033602 (2018).
  - [6] Pui-Wai Ma and S. L. Dudarev, “Universality of point defect structure in body-centered cubic metals,” *Phys. Rev. Materials* **3**, 013605 (2019).
  - [7] Murray S. Daw, Wolfgang Windl, Neil N. Carlson, Matt Laudon, and Michael P. Masquelier, “Effect of stress on dopant and defect diffusion in si: A general treatment,” *Phys. Rev. B* **64**, 045205 (2001).
  - [8] M. J. Aziz, “Pressure and stress effects on diffusion in si,” *Defect and Diffusion Forum* **153-155**, 1–10 (1998).
  - [9] P. H. Dederichs and K. Schroeder, “Anisotropic diffusion in stress fields,” *Phys. Rev. B* **17**, 2524–2536 (1978).
  - [10] C. N. Tomé, H. A. Cecatto, and E. J. Savino, “Point-defect diffusion in a strained crystal,” *Phys. Rev. B* **25**, 7428–7440 (1982).
  - [11] Céline Varvenne, Fabien Bruneval, Mihai-Cosmin Marinica, and Emmanuel Clouet, “Point defect modeling in materials: Coupling ab initio and elasticity approaches,” *Phys. Rev. B* **88**, 134102 (2013).
  - [12] D. M. Barnett, “The precise evaluation of derivatives of the anisotropic elastic Green’s functions,” *Physica Status Solidi (b)* **49**, 741–748 (1972).
  - [13] Emmanuel Clouet, Sbastien Garruchet, Hoang Nguyen, Michel Perez, and Charlotte S. Becquart, “Dislocation interaction with C in  $\alpha$ -Fe: A comparison between atomic simulations and elasticity theory,” *Acta Materialia* **56**, 3450 – 3460 (2008).
  - [14] G. Leibfried and N. Breuer, *Point Defects in Metals* (Springer Verlag, Berlin, 1978) p. 148.
  - [15] C. Domain and C. S. Becquart, “Ab initio calculations of defects in Fe and dilute Fe–Cu alloys,” *Phys. Rev. B* **65**, 024103 (2001).
  - [16] Céline Varvenne and Emmanuel Clouet, “Elastic dipoles of point defects from atomistic simulations,” *Phys. Rev. B* **96**, 224103 (2017).
  - [17] Yaakov Kraftmakher, “Equilibrium vacancies and thermophysical properties of metals,” *Physics Reports* **299**, 79 – 188 (1998).
  - [18] P.H. Dederichs, C. Lehmann, H.R. Schober, A. Scholz, and R. Zeller, “Lattice theory of point defects,” *Journal of Nuclear Materials* **69-70**, 176 – 199 (1978).
  - [19] W. Hertz, W. Waidelich, and H. Peisl, “Lattice contraction due to quenching in vacancies in platinum and gold,” *Physics Letters A* **43**, 289 – 290 (1973).

- [20] S.L. Dudarev, K. Arakawa, X. Yi, Z. Yao, M.L. Jenkins, M.R. Gilbert, and P.M. Derlet, “Spatial ordering of nano-dislocation loops in ion-irradiated materials,” *Journal of Nuclear Materials* **455**, 16 – 20 (2014), proceedings of the 16th International Conference on Fusion Reactor Materials (ICFRM-16).
- [21] G. Kresse and J. Hafner, “Ab initio molecular dynamics for liquid metals,” *Phys. Rev. B* **47**, 558–561 (1993).
- [22] G. Kresse and J. Hafner, “Ab initio molecular-dynamics simulation of the liquid-metal–amorphous-semiconductor transition in germanium,” *Phys. Rev. B* **49**, 14251–14269 (1994).
- [23] G. Kresse and J. Furthmüller, “Efficiency of ab initio total energy calculations for metals and semiconductors using a plane-wave basis set,” *Computational Materials Science* **6**, 15 – 50 (1996).
- [24] G. Kresse and J. Furthmüller, “Efficient iterative schemes for ab initio total-energy calculations using a plane-wave basis set,” *Phys. Rev. B* **54**, 11169–11186 (1996).
- [25] P. E. Blöchl, “Projector augmented-wave method,” *Phys. Rev. B* **50**, 17953–17979 (1994).
- [26] G. Kresse and D. Joubert, “From ultrasoft pseudopotentials to the projector augmented-wave method,” *Phys. Rev. B* **59**, 1758–1775 (1999).
- [27] John P. Perdew, Kieron Burke, and Matthias Ernzerhof, “Generalized gradient approximation made simple,” *Phys. Rev. Lett.* **77**, 3865–3868 (1996).
- [28] John P. Perdew, Kieron Burke, and Matthias Ernzerhof, “Generalized gradient approximation made simple [phys. rev. lett. 77, 3865 (1996)],” *Phys. Rev. Lett.* **78**, 1396–1396 (1997).
- [29] R. Hafner, D. Spišák, R. Lorenz, and J. Hafner, “Magnetic ground state of Cr in density-functional theory,” *Phys. Rev. B* **65**, 184432 (2002).
- [30] S. Cottenier, B. De Vries, J. Meersschant, and M. Rots, “What density-functional theory can tell us about the spin-density wave in Cr,” *Journal of Physics: Condensed Matter* **14**, 3275 (2002).
- [31] H. C. Herper, E. Hoffmann, and P. Entel, “Ab initio full-potential study of the structural and magnetic phase stability of iron,” *Phys. Rev. B* **60**, 3839–3848 (1999).
- [32] Pui-Wai Ma, S. L. Dudarev, and Jan S. Wróbel, “Dynamic simulation of structural phase transitions in magnetic iron,” *Phys. Rev. B* **96**, 094418 (2017).
- [33] Gregory Mills, Hannes Jansson, and Gregory K. Schenter, “Reversible work transition state theory: application to dissociative adsorption of hydrogen,” *Surface Science* **324**, 305 – 337 (1995).
- [34] Hannes Jónsson, Greg Mills, and Karsten W. Jacobsen, “Nudged elastic band method for finding minimum energy paths of transitions,” in *Classical and Quantum Dynamics in Condensed Phase Simulations* (World Scientific, 1998) pp. 385–404.
- [35] Yvon Le Page and Paul Saxe, “Symmetry–general least-squares extraction of elastic data for strained materials from ab initio calculations of stress,” *Phys. Rev. B* **65**, 104104 (2002).
- [36] Harry C. Nash and Charles S. Smith, “Single-crystal elastic constants of lithium,” *Journal of Physics and Chemistry of Solids* **9**, 113 – 118 (1959).
- [37] Charles Kittel, *Introduction to Solid State Physics*, 8th ed. (John Wiley & Sons, Inc., New York, 2004).
- [38] R. H. MARTINSON, “Variation of the elastic constants of sodium with temperature and pressure,” *Phys. Rev.* **178**, 902–913 (1969).
- [39] W.R. Marquardt and J. Trivisonno, “Low temperature elastic constants of potassium,” *Journal of Physics and Chemistry of Solids* **26**, 273 – 278 (1965).
- [40] E.J. Gutman and J. Trivisonno, “Temperature dependence of the elastic constants of rubidium,” *Journal of Physics and Chemistry of Solids* **28**, 805 – 809 (1967).
- [41] F.J. Kollarits and J. Trivisonno, “Single-crystal elastic constants of cesium,” *Journal of Physics and Chemistry of Solids* **29**, 2133 – 2139 (1968).
- [42] U. Buchenau, M. Heiroth, H. R. Schober, J. Evers, and G. Oehlinger, “Lattice dynamics of strontium and barium,” *Phys. Rev. B* **30**, 3502–3505 (1984).
- [43] M. W. Finnis and J. E. Sinclair, “A simple empirical N–body potential for transition metals,” *Philosophical Magazine A* **50**, 45–55 (1984).
- [44] S. B. Palmer and E. W. Lee, “The elastic constants of chromium,” *The Philosophical Magazine: A Journal of Theoretical Experimental and Applied Physics* **24**, 311–318 (1971).
- [45] J. A. Rayne and B. S. Chandrasekhar, “Elastic constants of iron from 4.2 to 300k,” *Phys. Rev.* **122**, 1714–1716 (1961).
- [46] P. Ehrhart, P. Jung, H. Schultz, and H. Ullmaier, *Landolt-Börnstein - Group III Condensed Matter · Volume 25: “Atomic Defects in Metals”*, edited by H. Ullmaier (Springer-Verlag Berlin Heidelberg, 1991).
- [47] D. Nguyen-Manh, A. P. Horsfield, and S. L. Dudarev, “Self-interstitial atom defects in bcc transition metals: Group-specific trends,” *Phys. Rev. B* **73**, 020101 (2006).
- [48] P. M. Derlet, D. Nguyen-Manh, and S. L. Dudarev, “Multiscale modeling of crowdion and vacancy defects in body-centered-cubic transition metals,” *Phys. Rev. B* **76**, 054107 (2007).
- [49] H. Schultz, “Defect parameters of b.c.c. metals: group-specific trends,” *Materials Science and Engineering: A* **141**, 149 – 167 (1991).
- [50] R. Benedek, L. H. Yang, C. Woodward, and B. I. Min, “Formation energy and lattice relaxation for point defects in li and al,” *Phys. Rev. B* **45**, 2607–2612 (1992).
- [51] R Pawellek, M Fahnle, C Elsasser, K M Ho, and C T Chan, “First-principles calculation of the relaxation around a vacancy and the vacancy formation energy in BCC li,” *Journal of Physics: Condensed Matter* **3**, 2451–2455 (1991).
- [52] W. Frank, U. Breier, C. Elsässer, and M. Fähnle, “Properties of monovacancies and self-interstitials in bcc li: An ab initio pseudopotential study,” *Phys. Rev. B* **48**, 7676–7678 (1993).
- [53] W. Frank, U. Breier, C. Elsässer, and M. Fähnle, “First-principles calculations of absolute concentrations and self-diffusion constants of vacancies in lithium,” *Phys. Rev. Lett.* **77**, 518–521 (1996).
- [54] U. Breier, W. Frank, C. Elsässer, M. Fähnle, and A. Seeger, “Properties of monovacancies and self-interstitials in bcc na: An ab initio pseudopotential study,” *Phys. Rev. B* **50**, 5928–5936 (1994).
- [55] V. Schott, M. Fähnle, and P. A. Madden, “Theory of self-diffusion in alkali metals: I. results for monovacancies in li, na, and k,” *Journal of Physics: Condensed Matter* **12**, 1171–1194 (2000).
- [56] George H. Vineyard, “Frequency factors and isotope effects in solid state rate processes,” *Journal of Physics and Chemistry of Solids* **3**, 121 – 127 (1957).



- [57] S. L. Dudarev, “Coherent motion of interstitial defects in a crystalline material,” *Philosophical Magazine* **83**, 3577–3597 (2003).
- [58] Sergei L. Dudarev, Daniel R. Mason, Edmund Tarleton, Pui-Wai Ma, and Andrea E. Sand, “A multi-scale model for stresses, strains and swelling of reactor components under irradiation,” *Nuclear Fusion* **58**, 126002 (2018).
- [59] U. Breier, V. Schott, and M. Fähnle, “Ab initio calculation of formation and migration volumes for vacancies in li and na,” *Phys. Rev. B* **55**, 5772–5777 (1997).
- [60] R. A. Hulthsch and R. G. Barnes, “Pressure dependence of self-diffusion in lithium and sodium,” *Phys. Rev.* **125**, 1832–1842 (1962).
- [61] John N. Mundy, “Effect of pressure on the isotope effect in sodium self-diffusion,” *Phys. Rev. B* **3**, 2431–2445 (1971).
- [62] I. G. Margvelashvili and Z. K. Saralidze, “Influence of an elastic field of a dislocation on the steady state diffusion fluxes of point defects,” *Sov. Phys. Solid State* **15**, 1774–1776 (1974).
- [63] P. T. Heald, “The preferential trapping of interstitials at dislocations,” *The Philosophical Magazine: A Journal of Theoretical Experimental and Applied Physics* **31**, 551–558 (1975).